

Bending of CORC® cables and wires: finite element parametric study and experimental validation

V. A. Anvar^{1,2,3}, K. Ilin¹, K.A. Yagotintsev¹, B. Monachan^{1,3}, K.B. Ashok^{1,3}, B. A. Kortman¹, B. Pellen¹, T.J. Haugan⁴, J. D. Weiss^{5,6}, D.C. van der Laan^{5,6}, R. J. Thomas³, M. Jose Prakash³, M.S.A. Hossain^{2,7}, A. Nijhuis¹

¹ *The University of Twente, Faculty of Science & Technology, 7522 NB Enschede, the Netherlands*

² *Institute for Superconducting and Electronic Materials, University of Wollongong, Wollongong, Australia*

³ *Department of Mechanical Engineering, T.K.M. College of Engineering, India*

⁴ *US Air Force Research Laboratory, Wright Patterson AFB, OH 45433, USA*

⁵ *Advanced Conductor Technologies, Boulder CO 80301, USA*

⁶ *Department of Physics, University of Colorado, Boulder, CO 80309, USA*

⁷ *School of Mechanical and Mining Engineering, the University of Queensland, Brisbane, QLD 4072, Australia.*

Abstract

A CORC® cable is composed of several layers of helically wound high-temperature superconducting (HTS) tapes on a round core with the winding direction reversed in each successive layer. The cable is flexible but the flexibility is limited by the critical strain value causing breakage of the HTS layer when this strain level is exceeded. The cables for magnets in fusion reactors experience large mechanical and electromagnetic loads. These loads arise from the cabling, coil manufacturing, cooling, and magnet operation. In order to optimize the manufacture and operating conditions, the mechanical behavior of CORC® cables must be understood for the different relevant loading conditions. The cable configuration with many contact interactions between tapes and the non-linear behavior of the materials during the production and operating conditions makes the modeling challenging. Detailed finite element (FE) modeling is required to account for these complexities. The FE modeling allows an accurate calculation of the stress-strain state of the cable components under various loads and avoids time-consuming large-scale experimental optimization studies. This work presents a detailed FE modeling of the 3D stress-strain state in a CORC® wire under bending load. The elastic-plastic properties of the individual tape composite materials and its temperature dependence are taken into account. The FE model is experimentally validated by a multi-layer CORC® bending test performed by Advanced Conductor Technologies LLC. A critical intrinsic tensile strain value of 0.45% is taken as the threshold where the individual tape performance becomes irreversibly degraded.

The proposed FE model describes the bending test of the CORC® wire adequately and thus can be used to study other types of loads. A parametric study is ongoing with dependent variables to pursue a further optimization of CORC® cables and wires for various applications.

Keywords: CORC cable, REBCO, HTS, finite element method, numerical simulation, composite beam bending, superconductivity

1 Introduction

The state of the art of so-called second-generation (2G) HTS tape, also known as coated conductors, is typically a 100 μm thick composite tape, in which a layer of superconducting material ($\sim 1\text{-}2\ \mu\text{m}$) is grown on a solid substrate and then coated with a copper layer for stabilization. The superconducting layer is made of a rare-earth element, brittle ceramic material. In contrast with the low-temperature superconducting (LTS) round wires, commercially produced RE-Ba₂Cu₃O_{7- δ} (RE = Rare Earth) coated conductors are only available as tapes. This gives complications when large transport currents are required and hence a cable should contain many tapes. As

an example, fusion or accelerator magnet coils require high current conductors to limit their self-inductances. Three main cable concepts based on REBCO tapes are being developed: Conductor on Round Core (CORC®), Twisted Stack-Tape Cables (TSTCs) and Roebel Coated Conductor Cables (RACCs) [1] - [3]. Other variants of stacked tape concepts are also under development [3] [5]. The key features differentiating various cabling concepts are methods of transposition, utilization, and assembly of tapes. Among them, only CORC® cable has the combined features of relatively high current, high current density, and high isotropic flexibility.

The circular cross-section of CORC® conductor enables easy implementation of the partial transposition of multiple bundled tapes. The core former, mostly chosen to be made of copper, provides an often-desirable percentage (25% to 50%) of stabilizer but reduces the cable effective area available for superconducting current transfer resulting in lower engineering current density than could be obtained by other cabling methods. However, a record current density of 344 Amm⁻² at 4.2 K and 17 T has recently been demonstrated in a CORC® cable [6]. Reduced substrate thickness and width of the REBCO tapes allows the production of much thinner CORC® cables, called wires, as thin as 3 mm in diameter with the potential to enhance the engineering current density and flexibility further [7]. CORC® cables and wires are being developed for the next generation of accelerator magnets because of their high flexibility and potential for high engineering current densities [8].

The critical current in REBCO tapes is strain dependent. The strain in the tapes within CORC® cables and wires arises from the tape production process (thermal strain), cable production (winding strain), magnet winding of cable (bending strain), cooling (thermal strain), and electromagnetic forces during operation (strain from transverse and hoop loads). The stress-strain characteristics under tensile, torsional and transverse loads of single tape are extensively studied by experiments and FE modeling and published elsewhere [9]. This previous research on single tapes forms the basis for the present study and CORC® model development. A similar study on the numerical and experimental investigation of the electromechanical behavior of REBCO tapes under only tension and combined tension-torsion was performed in [10].

Electro-mechanical analysis by analytical, FEM and experimental methods on the main cabling configurations other than CORC® was already reported in [11]. This study aims at analyzing the strain in the REBCO layer during winding and bending of CORC® cables and wires as the first step in design optimization. Analysis of cable bending characteristics is important since magnet winding always involves cable deformation to various radii of curvature. The bending diameter at which, the critical current starts to degrade irreversibly, is called the critical bending diameter. This diameter depends on the parameters like the diameter of the conductor core, number of layers, winding angle, winding tension, tape width, tape thickness, the coefficient of friction between tapes (multilayer cables), and coefficient of friction between tape and core. Generally speaking, a smaller core diameter, lower number of tape layers and smaller twist pitch will induce a larger tape strain during cable winding alone and a lower strain during bending alone. Optimization of design variables can be performed to improve the mechanical behavior of the CORC® cable. This paper is divided into four main sections describing first the details of the FE model, second the experimental validation of the FE model, third some results of a parametric study and related discussions and finally the conclusion.

Superconducting cables are widely used in low inductive high field magnet systems that require conductors with high current capabilities. The CORC® cable concept has a great potential for many applications but particularly in very large magnet systems such as in fusion reactors to generate clean and safe energy. The ITER fusion reactor, presently being built in France, relies on LTS materials. The next fusion reactors (DEMO or ARC) [14 - 15], could highly benefit from HTS magnet system providing a higher operating temperature or at least a larger temperature operating margin, more compact magnets and a simpler cryostat, resulting in substantial cost savings.

2 Finite element modeling

The goal of CORC® cable and wire FE bending simulation is to calculate the stress-strain state (SSS) of all the materials within the cable. The conductor critical current degradation can be calculated as a function of bending diameter if the strain in the REBCO layers is known as a function of the bending diameter. The cable materials already have some non-zero intrinsic strains before applying the bending load. These strains are imposed due to the cumulative effect of the production process from individual tape and the production of the cable (tape winding on the core) itself. In order to take into account these initial strains, we model two consecutive processes: the tape production process and the cable production process.

A CORC® cable or wire consists of several layers of tapes. Since the tapes from each layer of the cable have different SSS due to the different winding angle and diameter, the SSS of the tape is calculated for each layer at the beginning. Thus we create N finite-element models, where N is number of cable layers. Each of N models consists of two steps: the tape production process accounting for the residual strain in the REBCO material [18] build up during the tape production process and the winding process of the tape on to a cylinder whose diameter is

$$D_i = D_{CORE} + 2 \cdot (i - 1) \cdot H_{TAPE}, \quad i \in (1, N) \quad (1).$$

Where D_{CORE} is the core diameter, i is the layer number, H_{TAPE} is the tape thickness.

After the calculation for all N layers, we have the SSS for all tapes in all layers for the straight cable configuration. In the following step, we create the full straight cable mesh geometry, which is stress-free initially. Next, we assign the SSS from previous N calculations in the cable geometry as an initial strain condition. The SSS neglects accumulated transverse pressure in the layers since the winding tension has a small magnitude (8-10 N) and the sensitivity to transverse stress is marginal [9]. Thus we have created a straight cable model with the proper SSS as reached after the production process of the cable. Then the bending load is applied to the cable. The compressive strain on tape layers from cable bending alone is included in the simulation by default. The modeling steps are schematically shown in Figure 1.

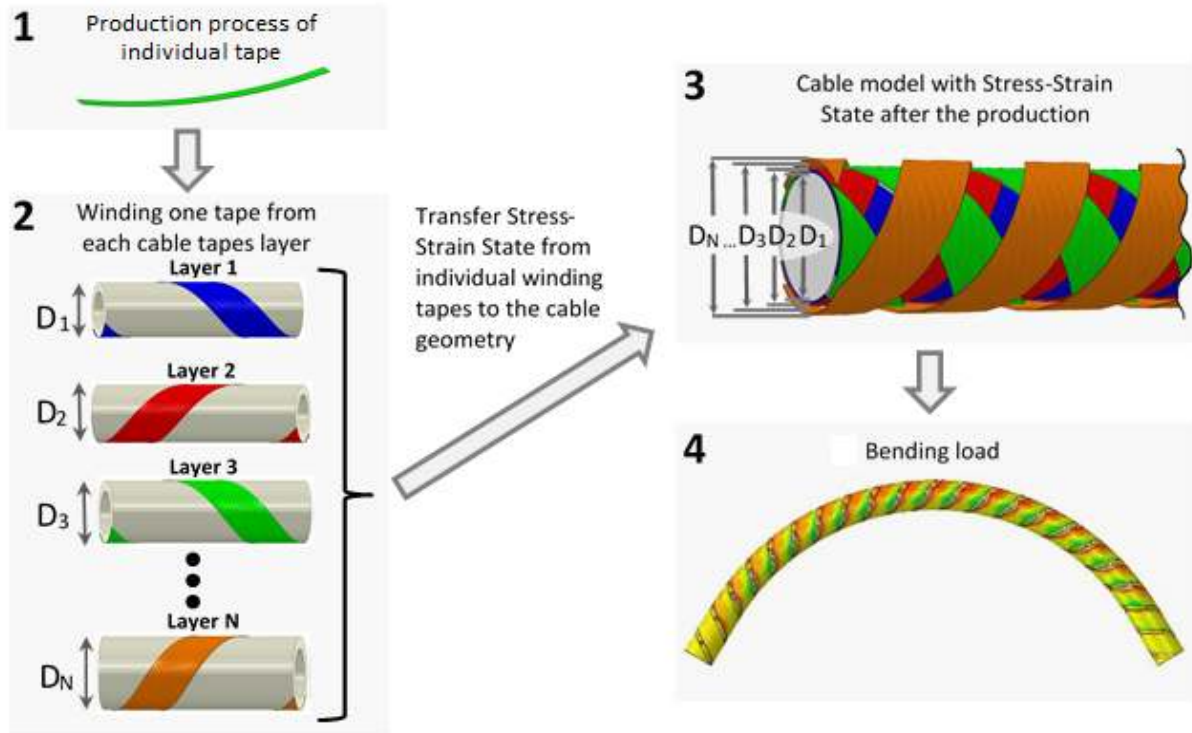


Figure 1. FEM cable bending modeling steps.

The stress-strain state of the cable is calculated for different bending diameters. The criterion of 0.45% tensile strain in the REBCO material is adopted as a threshold value for crack initiation [18]. It is assumed that areas of REBCO material with a tensile strain above 0.45% are damaged and have lost the superconducting properties. For convenience, it is also assumed that the dependency between the critical current and undamaged volume of superconducting material is linear. It can be argued that this can serve as a first-order approach, although in reality, this relation is more complex with dependency on current distribution in the REBCO layer, local strain distribution, crack traces and local magnetic field magnitude and orientation. However, the normalized critical current is here calculated as:

$$\frac{I_c}{I_{c0}} = 1 - \frac{V_{REBCO}^{Damaged}}{V_{REBCO}} \quad (2)$$

Where, I_c/I_{c0} is the normalized critical current, V_{REBCO} is the volume of all REBCO material in the cable, $V_{REBCO}^{Damaged}$ is the volume of damaged REBCO material (tape intrinsic tensile strain has exceeded 0.45%).

2.1 Step 1 – Tape production process

Figure 2 shows the configuration of the SuperPower 2G HTS tape, which is used for all tape and cable experiments and modeling. The tape structure can vary in width and thickness of the composite materials. The tape identification number used by SuperPower is SCS#### where the first # denotes the width in mm and the last three # denote the thickness of the Hastelloy substrate in μm .

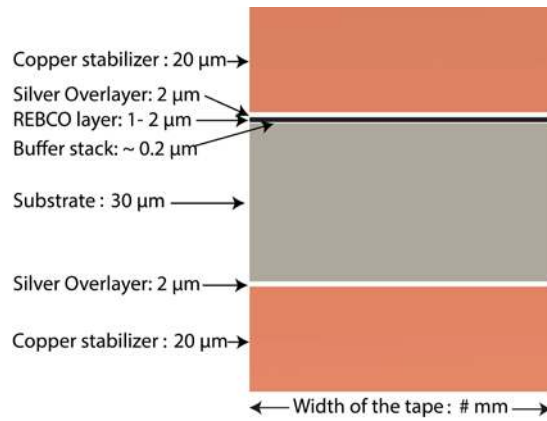


Figure 2. Configuration of SuperPower 2G HTS Tape SCS#030

It is necessary to model the entire tape production process to know the residual strain originated in the REBCO layer, which can be up to approximately 50% of the critical strain depending on the type of the tape. The modeling of the tape production process was described in detail in [9]. There are some differences between the published model and the present model. These differences concern dissimilar types of finite elements and boundary conditions. In the present model, a general purpose layered shell elements S4R¹, 4 noded quadrilateral stress-displacement shell element with reduced integration is used. Due to the high aspect ratio (width/thickness) of the REBCO tapes this plane stress assumption is more reliable from a computational point of view. This is a 4-node reduced integration finite element with one integration point by area. Also, 4 layers are assigned to this element having an individual thickness and material properties (two Copper layers, REBCO and Hastelloy). The thickness of each layer varies depending upon the manufacturer's design specification. Each layer has three integration points by thickness. Thus each composed element has 12 integration points by thickness, which allows calculating the SSS over the tape.

The material properties used for the simulation are given in Table 1.

Table 1. Material properties of Hastelloy, copper, and REBCO [9].

	Young's modulus (GPa)	Yield stress (MPa)	Poisson ratio	Thermal expansion coefficient (K ⁻¹)
Hastelloy (RT)	223	891	0.307 [23]	1.34×10^{-5} [18]
Hastelloy (77 K)	228	1141	0.307 [23]	1.34×10^{-5} [18]
Copper (RT)	80	120	0.34 [24]	1.77×10^{-5} [18]
Copper (77 K)	98	146	0.34 [24]	1.77×10^{-5} [18]
REBCO	157 [25]	-	0.30 [25]	1.10×10^{-5} [18]

Artificial properties are assigned to the copper layers for the first step of tape modeling involving the initial temperature decrease because the copper at that stage is not present yet. The first step simulates the MOCVD (metal organic chemical vapor deposition) on the buffered IBAD (ion beam assisted deposition) template. During this process, the temperature of the tape decreases from 1020 to 350 K. The copper is assumed to have a very high degree of plasticity that does not affect the SSS of the remaining materials. The artificial young's modulus used to provide a high degree of plasticity in the initial step is 1E-8 GPa. The artificial copper properties are then replaced by typical properties for simulation of the Cu-electroplating process and the second temperature step

¹ ABAQUS™ documentation.

lowering the temperature from 350 K to room temperature (293 K). Modeling steps for the production process of the REBCO composite tape are shown in Figure 3.

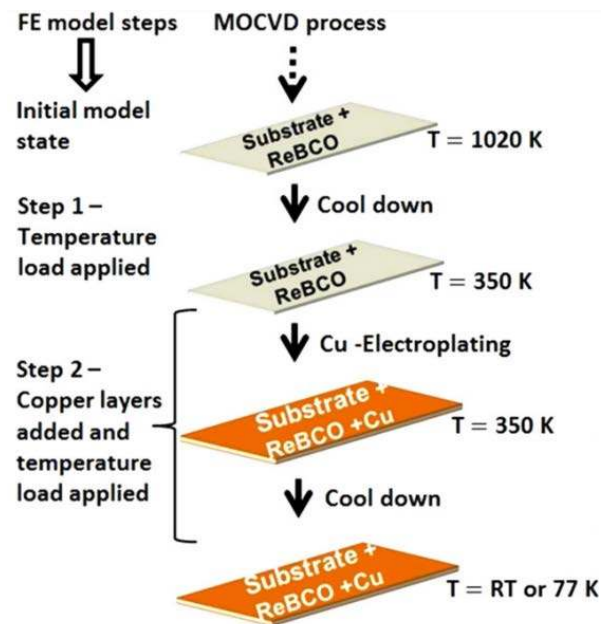


Figure 3. FE modeling steps for REBCO tape production process [9].

Figure 4 shows the specimen geometry. This geometry has a parallelogram shape, which is more convenient for the implementation of the winding process modeling. The mesh of this specimen has 12 elements along the tape width.

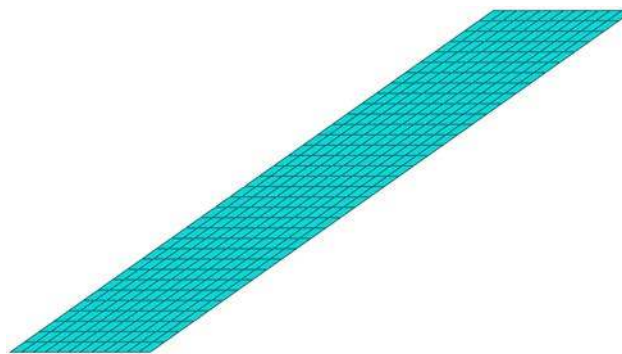


Figure 4. Tape mesh of the tape (top view).

The calculation of the compressive strain in the REBCO layer at room temperature gives about -0.15% for SCS2030 tape. For the winding model, we use the SSS of the tape after the production process at 293 K as an initial condition.

2.2 Step 2 – Winding individual tape

During this step, the tape specimen is wound around the core (Figure 5). This step is repeated for one tape from each layer. This step provides data on the stress and strain components from 12 finite elements across the tape for each chosen tape layer (Figure 5).

Then the core, which is a solid tube, is added to the model. An eight-node cubic-like element with reduced integration, C3D8R² is used for the mesh of the core. The created mesh has 1 element by the thickness and 48 elements by circumference. The diameter of the cylinder for each layer is calculated by formula (1).

The boundary condition for the winding model is shown in Figure 6 and it includes the SSS of the tape from the production process. For the contact between core and tape surfaces a friction coefficient of 0.2 is taken. It should be noted that the friction coefficient has hardly any influence on the SSS of the tape during the winding. In this model, only one twist pitch is used for winding. The angle between tape and the core axis is the same as for the cable that has been experimentally tested.

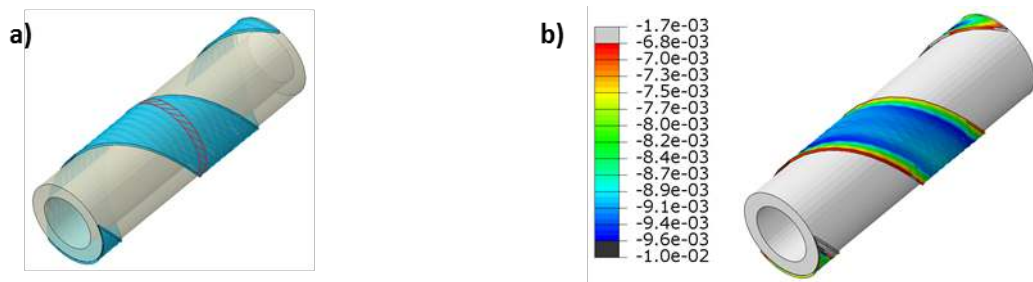


Figure 5. a) Deformation state after winding. b) Distribution of the principal strain in the REBCO layer after winding.

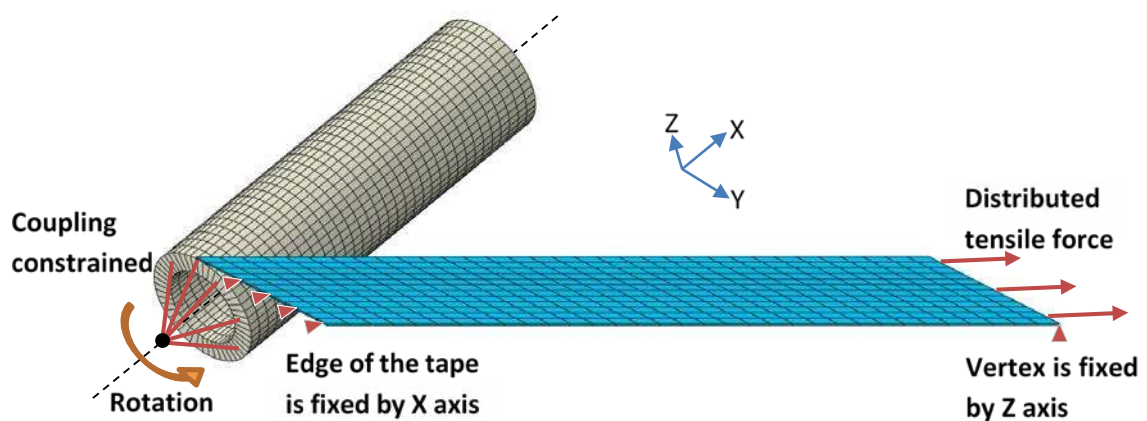


Figure 6. Boundary conditions and loads for the winding model.

As a result of this step, the SSS of the tapes from each cable layer is obtained. Figure 7 shows the distribution of various components of strain across the tape after the tape production process and after the winding for the SCS2030 tape having 2 mm width, 3.2 mm core diameter, 8 N applied tensile winding force and a winding angle of 45° as an example.

² ABAQUS™ documentation.

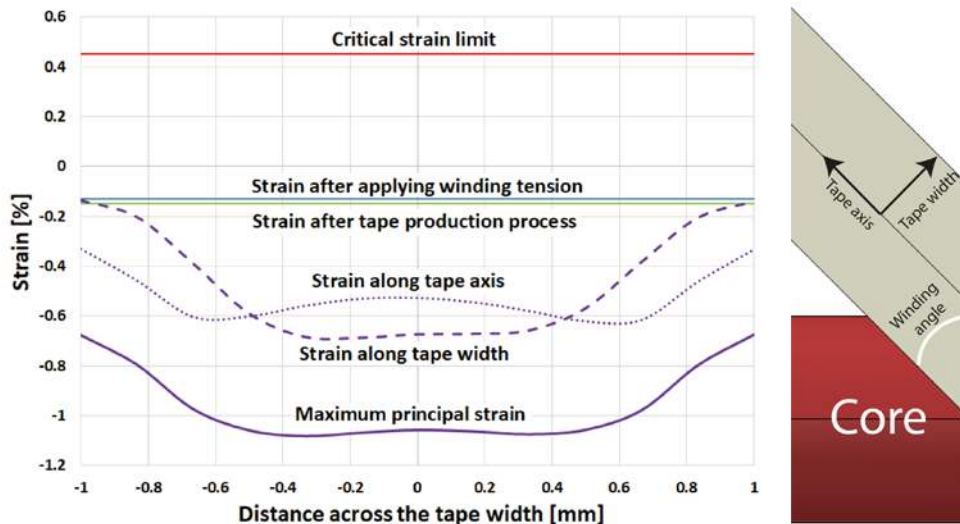


Figure 7. Strain components in the REBCO layer after the sequential modeling steps.

The REBCO strain after the production process (-0.15%) and after applying the tensile force (-0.13%) is uniform across the tape. After cable winding, the strain significantly decreases and becomes non-uniform. The lower compressive strain at the edges of the tape can be explained by the free boundaries and the actual shape of the tape [19]. The complex multilayer interaction of matrix materials during the winding, results in peak tape axial strain in the center of the tape. This peak also depends on the aspect ratio of the tape. For tapes with larger width, the bump flattens out. The strain distribution along the width causes a corresponding critical current spread as well. It should be noted that the tape is wound with the REBCO layer facing to the core (see Figure 2). Therefore after winding the net strain in the REBCO layer is more compressive than after the tape production process. The strain components for tape length and width are practically in the same range for a winding angle of 45°.

2.3 Step 3 – Cable production process; composition of the tape layers

Here the FE cable model is completed in which every tape has the SSS as after the cable winding process. As a first step, the geometry of the complete cable is created containing all tapes and the core as individual parts as shown in Figure 8. For all contacting surfaces, a contact interaction with a defined friction coefficient is assigned. A simple friction model is assumed in which the friction coefficient does not depend on other factors, such as temperature, contact stress etc.

Then the FE mesh is created for each part and the size of the finite elements in the tape of each tape layer is the same as in the tape-winding model of the corresponding layer described in the previous section. As a boundary condition, we create a kinematic coupling constraint on each end of the cable. Kinematic coupling constraints are used when a group of nodes can be constrained to the motion of a rigid body defined by a reference node. This will allow the plane section of the cylinder end to remain planar. These constraints define and connect the end edges of all tapes and end face of the core with one reference point. A prescribed rotation of one complete revolution is given to the reference node while constrained in the translational degree of freedom.

The material properties are obviously the same as used for creating the windings with the individual tape model. Then for each finite element and for each integration point of the element, we assign three stress components: S_{11} , S_{22} and S_{12} , three components of plastic strain: ε_{11}^{pl} , ε_{22}^{pl} and ε_{12}^{pl} and one component of equivalent plastic

strain ε_{eq}^{pl} , as initial conditions. These values are assigned in a local coordinate system, which is individual for each finite element. It should be noted that these 7 stress and strain components fully describe the elastic-plastic stress-strain state of the shell finite element. In the next step, we add the bending load in this model.

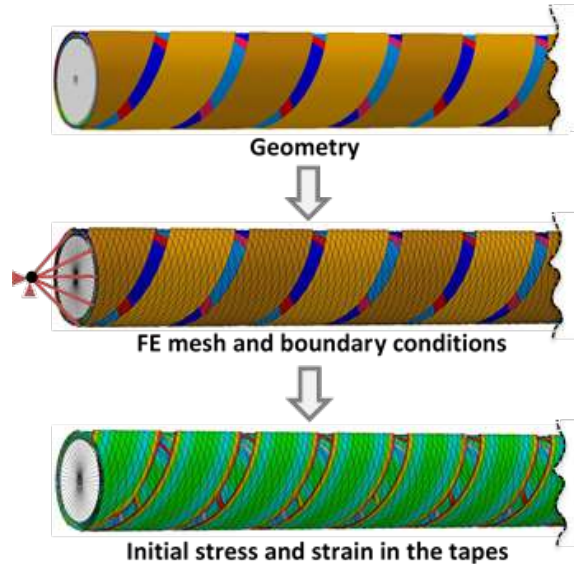


Figure 8. Steps sequence for creating the full cable model.

2.4 Step 4 – Cable bending

A quasi-static calculation is performed on the cable after transferring the SSS of all tape layers from the previous steps. Applying a specific bending load to the cable gives the corresponding SSS of the cable elements. Using the criterion of 0.45% strain in the REBCO material, the volume of damaged REBCO material due to the bending can be calculated. Figure 9 illustrates the boundary conditions used for the cable-bending model.



Figure 9. Boundary conditions for the cable bending model.

For the bending model, two kinematic coupling constraints were added in the core, placed at a small distance (~0.3 mm) from the ends of the cable. The rotation boundary conditions are applying to the reference points of these coupling constraints in opposite directions. The end sections of the cable are not subjected to bending, just as in the experimental setup that will be used later for bending studies with parametric cabling variations. This is done in order to avoid the influence of boundary conditions at the ends of the cable, which could lead to incorrect strain near the ends of the cable.

The strain field in the REBCO material as a result of a quasi-static calculation of the SSS in the bent cable is shown in Figure 10. Gray color denotes areas in which the principal strain component or the net strain exceeds the critical value of 0.45%. Thus we can calculate the number of damaged finite elements representing the volume with critical current degradation by formula (2). Although the estimation of the critical current degradation is qualitative, since also the strain and self-field plays a role, the minimum bending diameter where the first damage in the REBCO layer occurs is obviously by far most critical for applications.

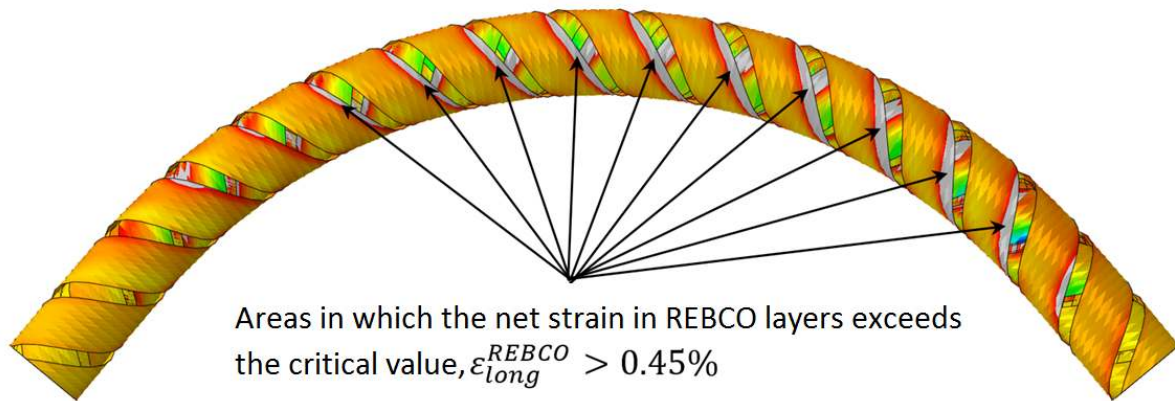


Figure 10. Distribution of the strain in the REBCO material during bending. The gray area has a strain above 0.45%.

3 FEM model comparison with experiment

The following experiment, performed by Advanced Conductor Technologies LLC (ACT), is taken as a reference for validation of the model computations. Figure 11 shows the structure of the CORC® wire.

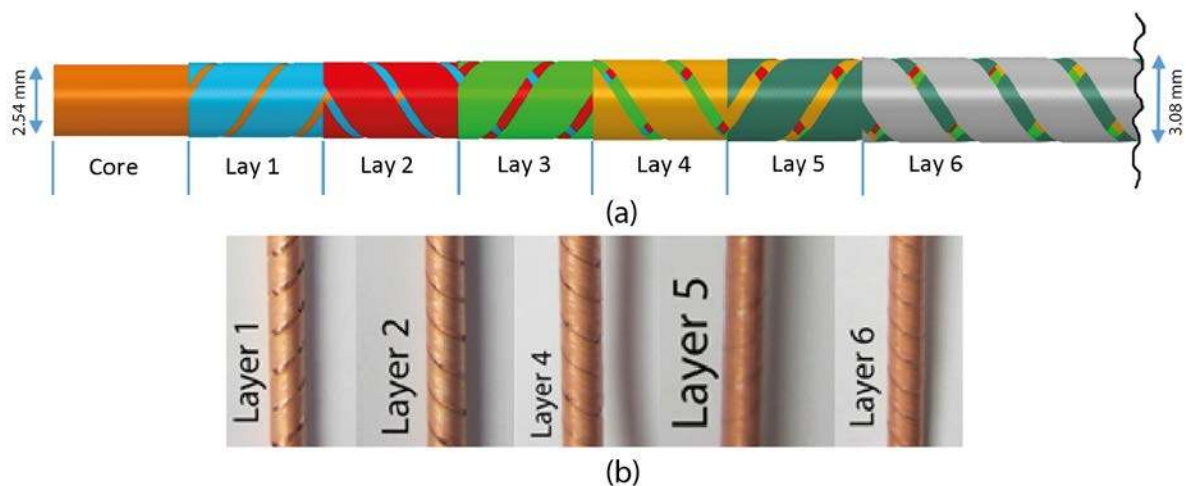


Figure 11. (a) Schematic structure and (b) actual pictures (no actual picture available for layer3) of the 6 layer CORC® wire.

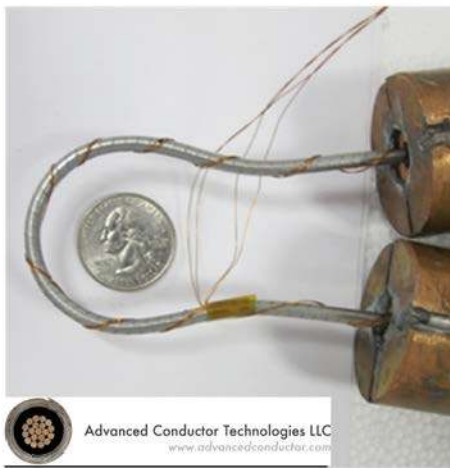
The CORC® wire consists of 6 layers of 2 mm wide REBCO tapes with 2 tapes per layer. The thickness of the REBCO layer, substrate, and copper plating used for the FE model are 1, 30, and 7 μm respectively. The actual thickness of the SCS2030 tape can vary from 42 to 46 μm since it includes buffer stack, silver cap layer, and YBCO in addition to Cu and substrate. For calculating the cylindrical diameter in obtaining the SSS in the winding,

the total thickness of the tape used in equation (1) is $45\ \mu\text{m}$. The calculated inner winding diameter (ID) is given in Table 2. The average twist pitch of the tape layers is 5.54 mm. The tensile force applied on the tape during winding is about 5 N. An additional gap ($\sim 5\ \mu\text{m}$) between each layer can occur in the wire due to the addition of lubricant during winding, but for the model, this variation is neglected. One of the dominating factors in determining the critical bending diameter of a cable or wire is the value of the coefficient of friction, which is unknown. The actual CORC® wire, with copper current terminations and voltage taps after bending, is shown in Figure 12 a. FEM prediction of critical bending diameter for the various coefficients of friction is plotted in Figure 12 b. After modeling with different values of coefficient of friction, the fitted value is 0.2, which seems credible since for the winding a lubricant is used. The details of all 6 layers of the CORC® wire is given in Table 2.

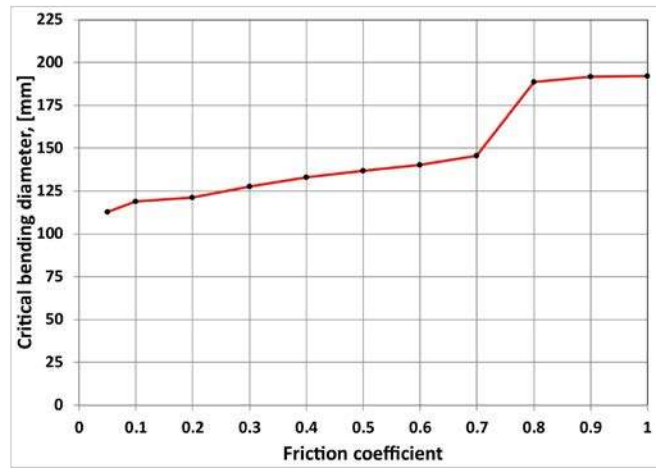
Table 2. Details of 6 layer CORC wire used in experimental validation.

Layer	ID[mm]	Gap[mm]	Pitch[mm/rev]	Angle[degrees]	Tape/mm wire
1	2.54	0.30	5.631	35.21	1.734
2	2.63	0.30	5.540	33.84	1.796
3	2.72	0.30	5.461	32.58	1.857
4	2.81	0.30	5.391	31.41	1.919
5	2.90	0.40	5.647	31.79	1.898
6	2.99	0.40	5.584	30.73	1.957

Details of the experiment and CORC® wire structure are explained in [7]. The outer diameter (OD) of the wire excluding outer non-superconducting tape layers is 3.08 mm. The inner diameters (ID) for each layer are calculated from the superconductor (SC) tape thickness, which is $45\ \mu\text{m}$. Only superconducting tape layers (SC) are considered for the FEM simulation i.e., the last two $50\ \mu\text{m}$ thick stainless steel layers and polyester heat shrink tubing of $30\ \mu\text{m}$ thickness is not taken into account for the simulation so far. The winding angle is the angle between the tape axis and normal direction to the axis of the core.



(a)



(b)

Figure 12. (a) CORC® wire bent to 35 mm diameter (b) FEM simulation - Critical bending diameter for various coefficients of friction.

Figure 13 a shows the variation of electric field with transport current. The results of the experimental bending test and FEM computation are presented together in Figure 13 b. The reduction of I_c from self-field effect alone is normalized before bending. However, during bending, the nominal I_c is calculated without any further self-field correction [7]. That is to say, the I_c reduction from self-field effects are not included in the FEM simulation. The computation is done for irreversible REBCO volume damage and not for I_c (B). The FEM model indicates progressive damage to the REBCO layer with bending which is comparable to the reduction of I_c with bending. This means that the FEM model can now be used for qualitative prediction of the flexibility of CORC® cables and wires under bending load for various design parameters. However, it is important to note here that the value of the friction coefficient is one of the dominating factors in determining the critical bending diameter of the wire. Here, critical bending diameter is defined as the diameter in which the tape starts to undergo irreversible damage by exceeding the critical strain limit of 0.45%. The friction coefficient depends on the above-mentioned cabling conditions, used materials e.g. lubrication and may even locally vary when subjected to bending. This will be further investigated in the future.

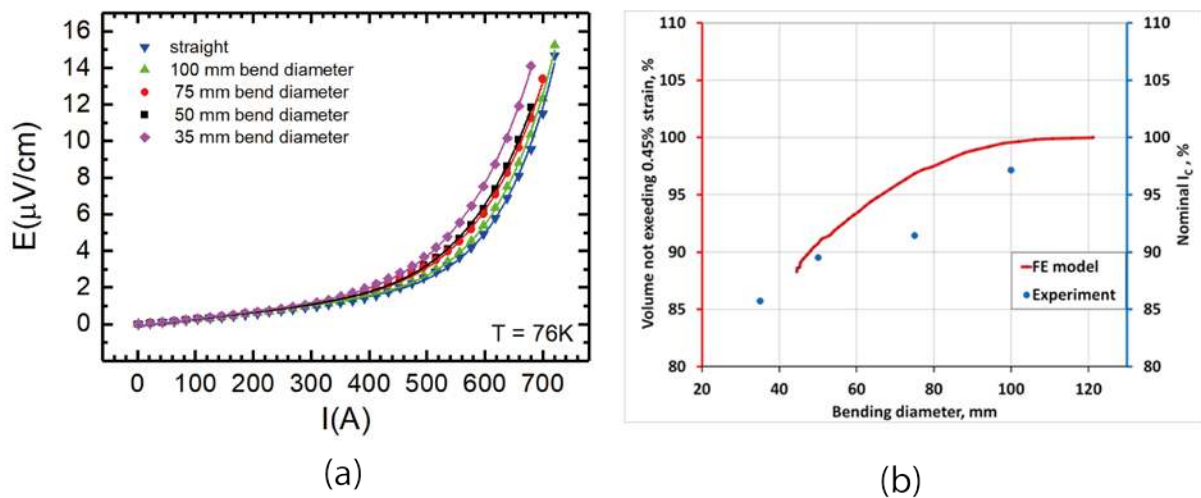


Figure 13. (a) E-I curve for various bending diameters [7] (b) Comparison of experimental I_c degradation and FEM damage propagation with bending for 6-layer CORC cable

4 Parametric study and discussions

4.1 Core diameter

It is obvious from the simple bending equation (3), to expect that the strain is at its maximum when the layer is furthest from the neutral axis of bending.

$$\varepsilon = \frac{-y}{d/2} \quad (3)$$

Where y is the distance to the neutral axis of bending and d is the bending diameter. Reducing the core diameter results in a reduction of y . This would mean that a smaller core diameter would result in a better flexibility of the cable. However, reducing of core diameter will result in higher compressive strain in the winding. Critical current reduces considerably with compressive strain but remains reversible at least up to -2% strain [16]. So there is a tradeoff between flexibility and critical current.

This expected behavior can be understood from the simulation results as shown in Figure 14. Here the critical bending diameter is plotted as a function of the friction coefficient for core diameters of 5, 6 and 7 mm.

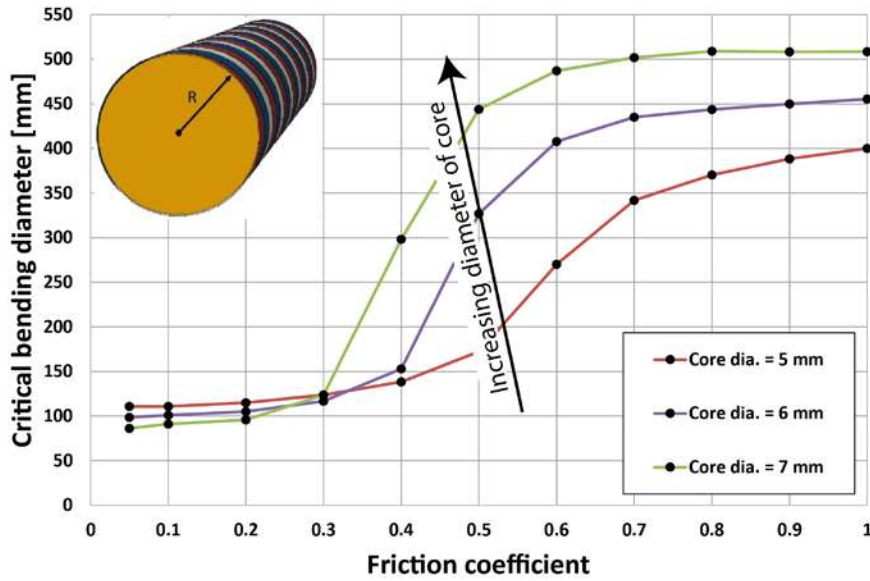


Figure 14. CORC® critical cable bending diameter as a function of friction coefficient upon varying core diameter.

However, the correlation between the smaller core diameter and higher cable flexibility depends highly on the friction factor. When the coefficient of friction reduces to below 0.3, the cable flexibility dependency on core diameter seems to vanish and be even slightly reversed. This behavior can be explained by stress relief in the tapes upon sliding between tapes and of tapes over the core. Local stress accumulation is minimized by sliding of the tape on the core. Sliding depends not only on friction coefficient but also on winding diameter, tape width, winding angle, etc. The observation made on friction coefficients in the range below 0.3 may not be valid for multilayer tapes or CORCs with different configurations.

4.2 Number of layers

Increasing the number of layers is to some extent analogous to increasing the core diameter. Figure 15 shows the expected trend with increasing number of tape layers.

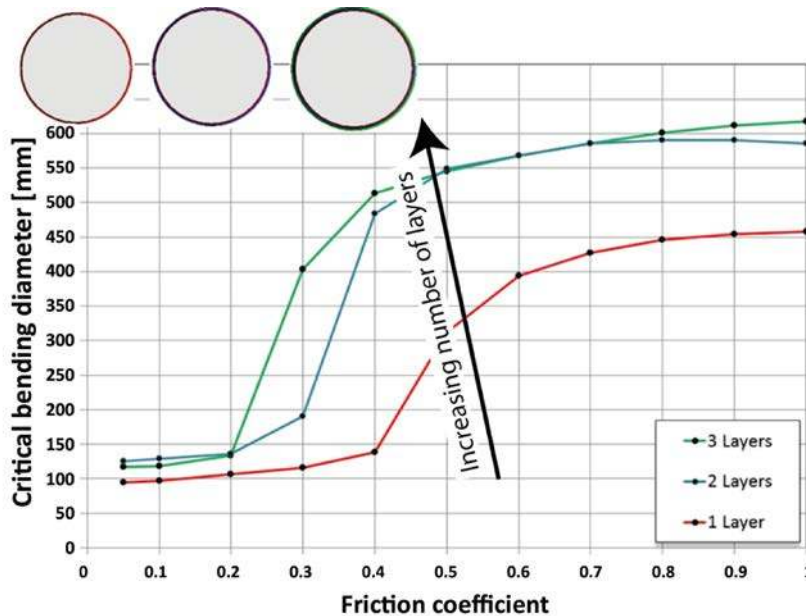


Figure 15. CORC® cable bending characteristics upon varying number of layers.

Note that there is a considerable gap in the bending curve of multilayer tape compared to a single layer tape. It is suggested that this could be due to increased restriction on sliding of the tapes over each other and the core. Also, the tapes in the inner layer experience a higher radial compression from the outer layers when multiple layers are present. The intersection of curves for 3 layers and 2 layers at around coefficient of friction 0.5 is the outcome of complex multilayer interactions, this may not be the case for another configuration.

4.3 Tape thickness

The tape thickness influences the choice of the core diameter in combination with the flexibility of CORC® cables. The tape is always wound with the REBCO layer facing the core, which results in a compressive strain in the REBCO layer, as shown in Figure 7. Changing the thickness of the Hastelloy substrate or of the surrounding copper layer can vary the thickness of the tape.

The outer Cu layer serves for electrical and thermal stability. For a single layer cable, the thickness of the Cu stabilizer almost doesn't influence the flexibility of the cable as shown in Figure 16. A single layer-SCS4030 tape is wound on a former with a diameter of 5 mm under a winding tension of 8 N and a winding angle of 45°. Nonetheless, the increase in the thickness of the Cu can reduce the overall flexibility of the cable as more and more layers are added. From a mechanical point of view, it is better to keep the Cu thickness as small as possible. The minimum Cu thickness of about 5 µm (on one side of the tape) is needed to completely cover the silver cap layer in preventing it from dissolving into the solder while making terminations [6]. Symmetrical deposition of Cu on both sides of the tape doesn't significantly change the position of the REBCO layer with respect to the neutral axis of the tape when bent around the central core. Hence the influence of the Cu stabilizer thickness on the winding strain in the REBCO layer is minimal. An asymmetric deposition of copper to keep the REBCO layer more closely to the neutral axis may reduce the winding strain in the REBCO layer.

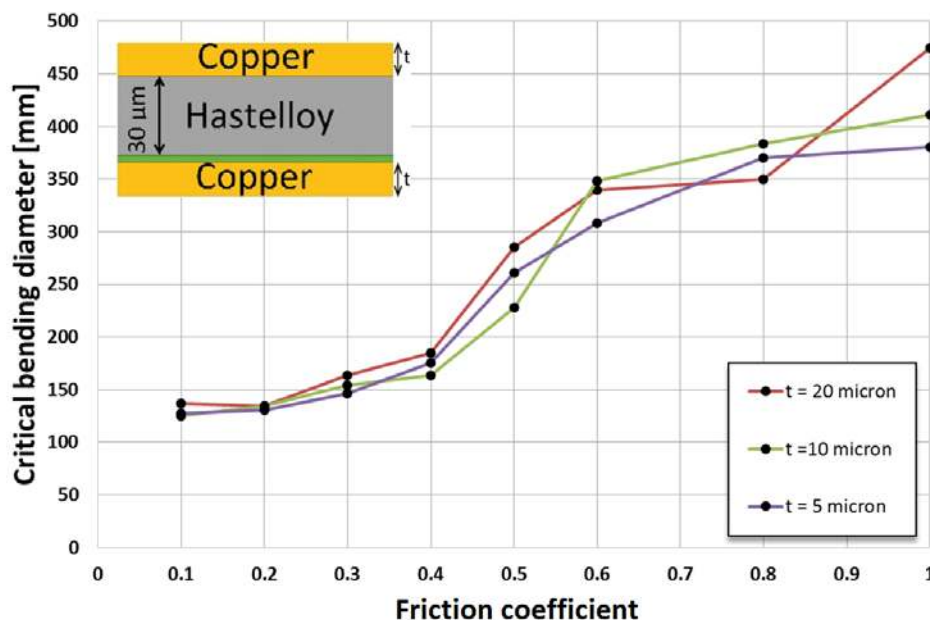


Figure 16. CORC® cable bending characteristics upon the varying thickness of the copper layer.

It is obvious that the REBCO layer thickness has much less influence on the flexibility of the cable due to its much smaller dimension compared with the thickness of the Hastelloy and copper. Increasing the thickness of the REBCO layer with required texturing is difficult but it can improve the tape critical current dramatically.

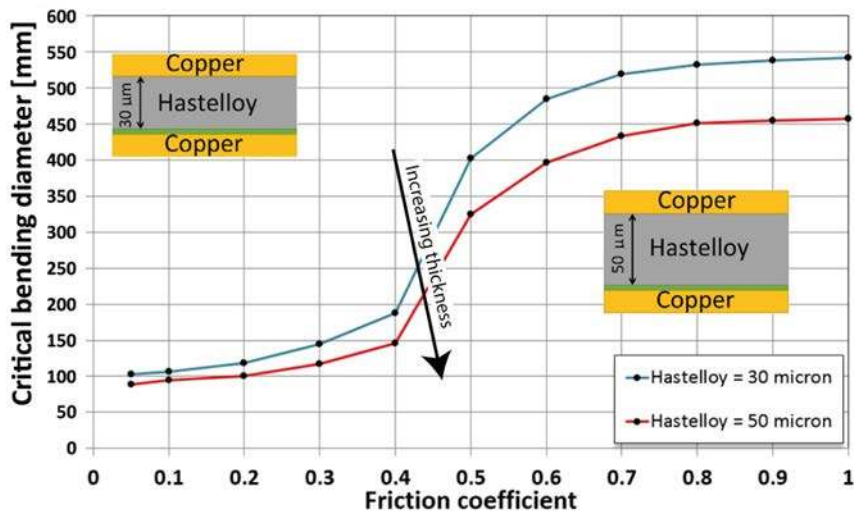


Figure 17. CORC® cable bending characteristics upon the varying thickness of Hastelloy substrate.

Larger Hastelloy thickness results in a higher compressive strain in the REBCO layer during winding. Higher compressive strain reduces the critical current but compressive strain remains reversible at least until -2% [7]. The tape with thinner Hastelloy layer reaches the irreversible tensile strain limit earlier when keeping the core diameter the same. So the cables with thicker substrate result in smaller critical bending diameter when the core diameter is kept constant. However, the minimum possible core diameter is determined by the maximum compressive strain in the tape during winding [7]. Tape with lower Hastelloy thickness can be wound on a smaller core which results in smaller critical bending diameter or increased flexibility, this is counter-intuitive to the behavior shown in Figure 17.

4.4 Winding angle

An interesting feature of REBCO tape in CORC® cable is its anisotropy in combination with the 0.45% critical tensile strain criterion. The winding angle is defined as the angle between the tape axis and axis perpendicular to the cable core. The winding angle dependency on the maximum strain in the REBCO layer during winding is infinitesimal; the strain generation from tape axial tensile force applied during winding is minimal. Smaller winding angle facilitates more tape movement over the core during bending allowing strain redistribution. So cables with larger tape winding angle tend to degrade faster as shown in Figure 18.

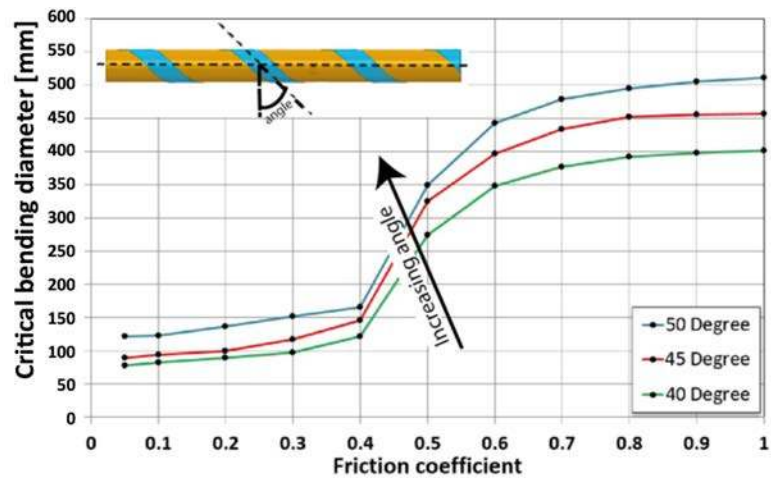


Figure 18. CORC® cable bending characteristics upon varying winding angle.

4.5 Tape Width

The AC loss in the conductor increases with the projected width (width normal to the magnetic field direction) of the REBCO tape. In this sense, although very marginal, decreasing the tape winding twist pitch in the cable can have a similar effect of reducing the projected width, hence the reduction of AC loss. However, reducing the width or striating the tape can reduce the AC loss in single tape configurations significantly [20], but the total AC loss of the cable is significantly influenced by the complex arrangement of tape layers. Also from the mechanical point of view, it can be shown that cables containing tapes with smaller width tend to be more flexible due to the increased ability to slide over the other tapes and core to reduce stress concentration. With increased tape width, the critical bending diameter gets less dependent on the friction coefficient and the bending response becomes more constant as shown in Figure 19. Here a single tape is wound on a former diameter of 2.55 mm under a winding tension of 8 N and a winding angle of 45°. The thickness of the tape, Cu and Hastelloy are 41, 5 and 30 μm respectively. The critical bending behavior of the tape from the FE results shows an irregular dependence with friction coefficient for various tape widths. The tapes with smaller width tend to slide more resulting in lower local stress accumulation. At a higher coefficient of friction, sliding of tape over the core is limited and the amount of tape damage is almost independent of tape width. Since the total amount of superconducting volume is lower for tapes with smaller widths, the percentage of damage will be more. The sliding nature of the tapes has rather a quite complex interaction for various tape widths. The overall effect is that tapes with a larger width are more flexible at higher friction coefficients and tapes with a smaller width are more flexible with lubrication or lower coefficient of friction. This may not be true for multilayered cable since additional layers reduce the sliding of tape due to increased friction. Experimental tests on simplified CORC® cabling configurations are needed to get a better understanding of this behavior.

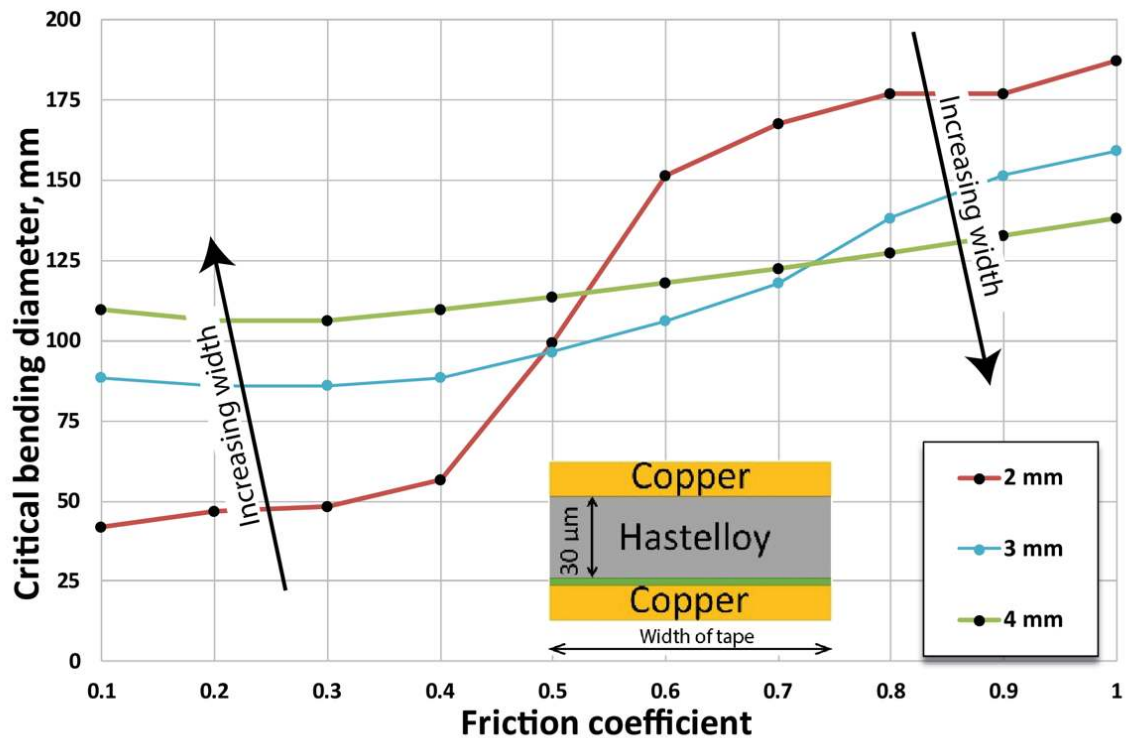


Figure 19. CORC® cable bending characteristics upon varying width of the tape.

5 Conclusion

A detailed CORC® FE model is built and a first validation is presented based on experimental data reaching a good qualitative agreement. Initial parametric studies have been performed that help to understand the cable bending behavior while varying geometrical parameters of the tape and cable. A reduced core diameter increases the flexibility and engineering current density but for this, tape with a smaller Hastelloy thickness is required. Further parameters that were investigated are copper stabilizer thickness, number of tape layers, winding angle and tape width. In all the parametric study cases, it is shown that reducing friction between tape(s) and core (by lubricating the tape during production) is a straightforward and effective way to increase the flexibility of the cable.

To further understand and optimize the cable model to reach a reliable quantitative level of prediction, extensive experiments are foreseen on simplified CORC cable configurations. As a next step to test the model, comparisons will be made of CORC® cables and wires experiments with parametric variations. In addition, other types of loads like cooling and Lorentz forces will be investigated to find the optimal configuration of CORC® cable and wire for various applications.

Acknowledgment

This work is supported in part by Eurofusion. Part of the work is also supported by the U.S. Department of Energy under contract numbers DE-SC0014009 and DE-SC0015775. Also supported by the Air Force Office of Scientific Research (AFOSR) LRIR #14RQ08COR, and the Aerospace Systems Directorate (AFRL/RQ) and by the Air Force Office of Scientific Research (AFOSR) LRIR # 18RQCOR100, and the Aerospace Systems Directorate (AFRL/RQ). The views and opinions expressed herein do not necessarily reflect those of any of the above-acknowledged parties.

References

- [1] Van der Laan DC, et al., 2013 “Characterization of a high-temperature superconducting conductor on round core cables in magnetic fields up to 20 T,” *Supercond. Sci. Technol.*, [10.1088/0953-2048/26/4/045005](https://doi.org/10.1088/0953-2048/26/4/045005)
- [2] Takayasu M, Chiesa L, Allen NC and Minervini J, 2016 “Present status and recent developments of the Twisted Stacked-Tape Cable conductor,” *IEEE Trans. Appl. Supercond.*, [10.1109/TASC.2016.2521827](https://doi.org/10.1109/TASC.2016.2521827)
- [3] Goldacker W, et al., 2014 “Roebel cables from REBCO coated conductors: a one-century-old concept for the superconductivity of the future,” *Supercond. Sci. Technol.*, [10.1088/0953-2048/27/9/093001](https://doi.org/10.1088/0953-2048/27/9/093001)
- [4] Celentano G, et al. 2014, “Design of an industrially feasible twisted-stacked HTS cable-in-conduit conductor for fusion application,” *IEEE Trans. Appl. Supercond.*, [10.1109/TASC.2013.2287910](https://doi.org/10.1109/TASC.2013.2287910)
- [5] D. Uglietti, R. Wesche, and P. Bruzzone, 2014 “Design and strand tests of a fusion cable composed of coated conductor tapes,” *IEEE Trans. Appl. Supercond.*, [10.1109/TASC.2013.2281783](https://doi.org/10.1109/TASC.2013.2281783)
- [6] Van der Laan D C et al 2016 Record current density of 344 Amm⁻² at 4.2 K and 17 T in CORC® accelerator magnet cables *Supercond. Sci. Technol.* [10.1088/0953-2048/29/5/055009](https://doi.org/10.1088/0953-2048/29/5/055009)
- [7] Jeremy D Weiss, Tim Mulder, Herman, J ten Kate, and Danko C van der Laan, 2017 Introduction of CORC® wires: highly flexible, round high-temperature superconducting wires for magnet and power transmission applications *Supercond. Sci. Technol.* [10.1088/0953-2048/30/1/014002](https://doi.org/10.1088/0953-2048/30/1/014002)
- [8] D C van der Laan, L F Goodrich, P Noyes, U P Trociewitz, A Godeke, D Abraimov, A Francis and D C Larbalestier 2015 Engineering current density in excess of 200Amm⁻² at 20T in CORC® magnet cables containing RE-Ba₂Cu₃O_{7-δ} tapes with 38µm thick substrates *Supercond. Sci. Technol.* [10.1088/0953-2048/28/12/124001](https://doi.org/10.1088/0953-2048/28/12/124001)
- [9] K Ilin, K A Yagotintsev, C Zhou, P Gao, J Kosse, S J Otten, W A J Wessel, T J Haugan, DC Van Der Laan and A Nijhuis, 2015 Experiments and FE modeling of stress–strain state in REBCO tape under tensile, torsional and transverse load, *Supercond. Sci. Technol.* [10.1088/0953-2048/28/5/055006](https://doi.org/10.1088/0953-2048/28/5/055006).
- [10] N C Allen, L Chiesa and M Takayasu 2015 Numerical and Experimental Investigation of the Electromechanical Behavior of REBCO Tapes IOP Conf. Series: Materials Science and Engineering [10.1088/1757-899X/102/1/012025](https://doi.org/10.1088/1757-899X/102/1/012025)
- [11] Makoto Takayasu, Luisa Chiesa, Leslie Bromberg and Joseph V Minervini 2012 HTS twisted stacked-tape cable conductor *Supercond. Sci. Technol.* [10.1088/0953-2048/25/1/014011](https://doi.org/10.1088/0953-2048/25/1/014011)
- [12] Nathaniel C. Allen, Federica Pierro, Zijia Zhao, Luisa Chiesa, and Makoto Takayasu 2017 Structural Finite Element Evaluation of Twisted Stacked-Tape Cables for High-Field Magnets *IEEE Trans. Appl. Supercond.*, [10.1109/TASC.2017.2652304](https://doi.org/10.1109/TASC.2017.2652304)
- [13] C Barth, K-P Weiss, M Vojenčiak and S Schlachter 2012 Electro-mechanical analysis of Roebel cables with different geometries *Supercond. Sci. Technol.* 25 [10.1088/0953-2048/25/2/025007](https://doi.org/10.1088/0953-2048/25/2/025007)
- [14] G. Federici et al 2017, “European DEMO design strategy and consequences for materials” *Nucl. Fusion* [10.1088/1741-4326/57/9/092002](https://doi.org/10.1088/1741-4326/57/9/092002)
- [15] ,B.N. Sorbom et al “ARC: A compact, high-field, fusion nuclear science facility and demonstration power plant with demountable magnets” *Fusion Engineering and Design* [10.1016/j.fusengdes.2015.07.008](https://doi.org/10.1016/j.fusengdes.2015.07.008)
- [16] Van der Laan D C, 2009 YBa₂Cu₃O_{7-δ} coated conductor cabling for low ac-loss and high-field magnet applications *Supercond. Sci. Technol.* [10.1088/0953-2048/22/6/065013](https://doi.org/10.1088/0953-2048/22/6/065013)
- [17] SuperPower® 2G HTS Wire Specifications http://www.superpower-inc.com/system/files/SP_2G+Wire+Spec+Sheet_for+web_2012FEC_v2_1.pdf
- [18] Osamura K, Sugano M, Machiya S, Adachi H, Ochiai S and Sato M 2009 Internal residual strain and critical current maximum of a surrounded Cu stabilized YBCO coated conductor *Supercond. Sci. Technol.* [10.1088/0953-2048/22/6/065001](https://doi.org/10.1088/0953-2048/22/6/065001)

- [19] Silas Alben, Bavani Balakrisnan, and Elisabeth Smela 2011 Edge Effects Determine the Direction of Bilayer Bending *Nano Letters - American chemical society*, [10.1021/nl200473p](https://doi.org/10.1021/nl200473p)
- [20] Francesco Grilli and Anna Kario 2016 How filaments can reduce AC losses in HTS coated conductors: a review *Supercond. Sci. Technol.* [10.1088/0953-2048/29/8/083002](https://doi.org/10.1088/0953-2048/29/8/083002)
- [21] Van der Laan D C et al 2011 Anisotropic in-plane reversible strain effect in $Y_{0.5}Gd_{0.5}Ba_2Cu_3O_{7-\delta}$ coated conductors *Supercond. Sci. Technol.* [10.1088/0953-2048/24/11/115010](https://doi.org/10.1088/0953-2048/24/11/115010)
- [22] C. Zhou, K. A. Yagotintsev, P. Gao, T. J. Haugan, D. C. van der Laan, and A. Nijhuis, Critical Current of Various REBCO Tapes Under Uniaxial Strain, *IEEE transactions on applied superconductivity*, [10.1109/TASC.2016.2535202](https://doi.org/10.1109/TASC.2016.2535202)
- [23] Special Metals Corporation 2004 Publication Number SMC019
www.specialmetals.com/files/alloys/inconel/Inconel%20alloy%20C-276.pdf
- [24] Freund L B and Suresh S 2003 *Thin Film Materials: Stress, Defect Formation, and Surface Evolution* (Cambridge: Cambridge University Press)
- [25] Cheon J H, Shankar P S and Singh J P 2005 Influence of processing methods on residual stress evolution in coated conductors *Supercond. Sci. Technol.* [10.1088/0953-2048/18/1/022](https://doi.org/10.1088/0953-2048/18/1/022)